Tectonophysics xxx (2010) xxx–xxx

Contents lists available at ScienceDirect

Tectonophysics

journal homepage: www.elsevier.com/locate/tecto

Late Triassic sinistral shear in the East Gobi Fault Zone, Mongolia

Laura E. Webb [a,*], Cari L. Johnson [b], Chuluun Minjin [c]

[a] Department of Geology, University of Vermont, Burlington, VT, USA
[b] Department of Geology and Geophysics, University of Utah, Salt Lake City, UT, USA
[c] Research Center for Stratigraphy and Paleontology, Mongolian University of Science and Technology, Ulaanbaatar, Mongolia

ARTICLE INFO

Article history:
Received 15 January 2010
Received in revised form 17 September 2010
Accepted 22 September 2010
Available online xxxx

Keywords:
Thermochronology
Intraplate deformation
Reactivation
Shear zones
Asia

ABSTRACT

Tectonic studies of the East Gobi Fault Zone in southeastern Mongolia reveal multiple, distinct intracontinental deformation events postdating late Paleozoic arc accretion and continental amalgamation. Metamorphic tectonites of the Tsagan Subarga and Tavan Har blocks, previously mapped as Precambrian basement, comprise a sinistral shear zone dominated by steeply-dipping, northeast-striking foliations. Field observations and petrographic analyses indicate that the protoliths of the metamorphic tectonites are Paleozoic arc volcanic and sedimentary sequences. $^{40}Ar/^{39}Ar$ step-heating analyses of minerals from pre-, syn-, and late- to post-kinematic lithologies bracket the timing of ductile sinistral shear as Late Triassic. The main phase of distributed deformation associated with cooling through amphibolite–upper greenschist-facies conditions occurred ca. 225 Ma and shear zone activity waned ca. 210 Ma. Cooling rates inferred from the $^{40}Ar/^{39}Ar$ data are on the order of 40–20 °C Myr^{-1}; apparent differences for the two basement blocks may reflect subsequent differential uplift during Late Jurassic–Cretaceous rifting. Relatively rapid Late Triassic cooling suggests a transtensional component to the deformation and is coincident with core complex formation in northern China. Late Triassic intraplate deformation in southeastern Mongolia is likely the result of far field forces associated with collision between Mongolian arcs and the Siberian craton (i.e. closure of the Mongol-Okhotsk ocean) and/or collisions associated with closure of the Paleotethys. The ductile shear zone has been documented over 250 km along strike and has been modified by subsequent brittle deformation events in the Mesozoic and Cenozoic.

1. Introduction

The East Gobi Fault Zone (EGFZ) is a structural corridor in southeastern Mongolia (Fig. 1). Areas within and adjacent to the EGFZ are well known for abundant mineral resources (e.g. the Oyu Tolgoi porphyry Cu–Au–(Mo) deposit; Perello et al., 2001). Despite being a region rich in mineral resources, tectonic models are largely speculative due the dearth of published studies and isotopic age constraints. Rocks in southeastern Mongolia are considered part of the Central Asian Orogenic Belt or Altaids and record the history of the amalgamation of Asia via collision and accretion in which micro-continental blocks are proposed to have played a significant role as a sight of nucleation (e.g. Sengor et al., 1993; Jahn, 1999). The geology of the EGFZ ultimately has implications for models of continental crustal growth and intracontinental deformation in Asia. Data from this region are important to constraining the relative roles of lateral extrusion versus continuum crustal thickening (e.g. Tapponnier et al., 1982; Houseman and England, 1993) related to intracontinental deformation associated with the collision of India with Asia. More broadly, constraints on the reactivation history of the EGFZ are beginning to reveal that deformation is temporally linked with Mesozoic–Cenozoic plate boundary processes and collisional orogenesis in Asia and potentially provides a long-term prediction of how shear zones and associated basins may evolve during continental growth.

The EGFZ has figured prominently into published models that hypothesize a kinematic linkage between the EGFZ and the Altyn Tagh Fault in China. Yue and Liou (1999) proposed a two stage model for the Altyn Tagh Fault: 1) ~400 km of sinistral offset in principally in the Oligocene with coeval slip on the EGFZ and associated faults to the northeast (i.e. lateral extrusion). 2) This phase of tectonic activity then transitions to shortening in Qilian Shan and Qaidam at 16–13 Ma (i.e. crustal thickening). This model contrasts with that of Lamb et al. (1999) who proposed 185–235 km sinistral offset along specific faults within the EGFZ (e.g. the Zuunbayan Fault) beginning in the Late Triassic to Early or Middle Jurassic based on the apparent offset of Paleozoic units (Fig. 2) and hypothesizing that some minor portion of the offset is likely associated with Cenozoic faulting. Similarities between the two models include sinistral offset inferred from map relationships between Paleozoic and older rocks; the principal difference between the two models is up to 400 km offset in Cenozoic versus ~200 km offset largely in the Mesozoic.

* Corresponding author. Department of Earth Sciences, Syracuse University, Syracuse, NY, USA. Tel.: +1 802 656 8136; fax: +1 802 656 0045.
E-mail address: lewebb@uvm.edu (L.E. Webb).

0040-1951/$ – see front matter © 2010 Elsevier B.V. All rights reserved.
doi:10.1016/j.tecto.2010.09.033

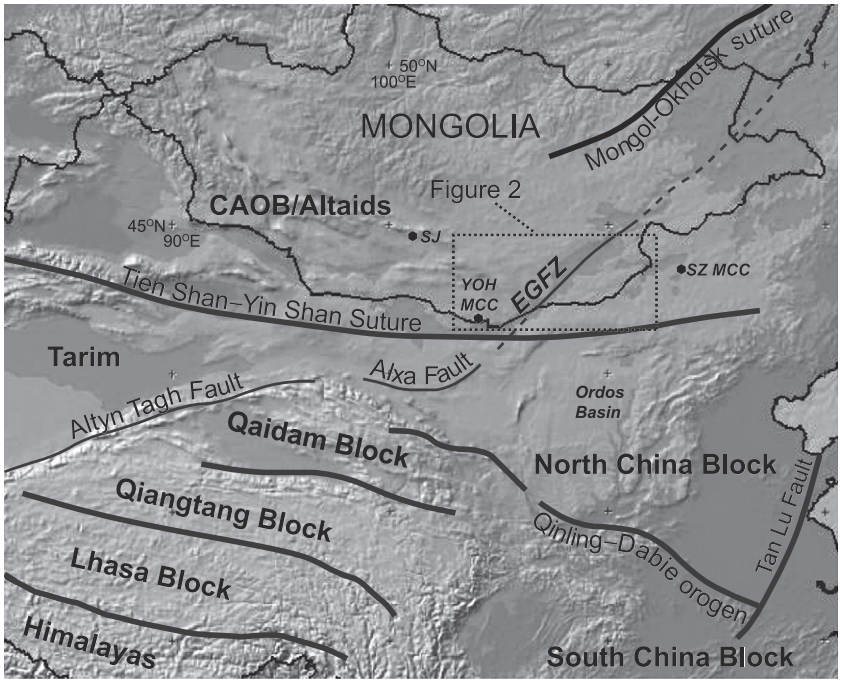

Fig. 1. Tectonic setting of the East Gobi Fault Zone (EGFZ). CAOB = Central Asian Orogenic Belt, YOH MCC = Yagan–Onch Hayrhan metamorphic core complex, SJ = Shin Jinst, and SZ MCC = Sonid Zuoqi metamorphic core complex. Background image created using GeoMapApp (www.geomapapp.org).

Subsequent to publication of these models, evidence for post-middle-Cretaceous movement on faults within the EGFZ was identified in seismic reflection data by Johnson (2004). Field evidence for Cenozoic deformation and faulting includes strike-slip faults and fracture sets that cut Upper Cretaceous and Cenozoic strata but lack evidence for neotectonic activity (Webb and Johnson, 2006). This Cenozoic phase of faulting and at least one Mesozoic phase of brittle deformation, Late Jurassic–Early Cretaceous rifting, both appear to locally exploit NE-striking structures associated with an early Mesozoic ductile sinistral shear zone. Pull-apart basins associated with the left-stepping, left-lateral Cenozoic fault system separate the fault-bounded basement blocks within the East Gobi Basin.

The metamorphic tectonites of basement blocks in the EGFZ have in many cases been traditionally mapped as Precambrian basement (e.g. Ruzhentsev and Pospelov, 1992; Tomurtogoo, 1999) based on their relatively high metamorphic grade and high strain. Until now, evidence for the early Mesozoic timing of this ductile deformation event has been limited to one $^{40}Ar/^{39}Ar$ analysis of biotite (~209 Ma, Lamb et al., 1999). We present data from fifteen $^{40}Ar/^{39}Ar$ step-heating analyses of minerals from pre-, syn-, and late- to post-

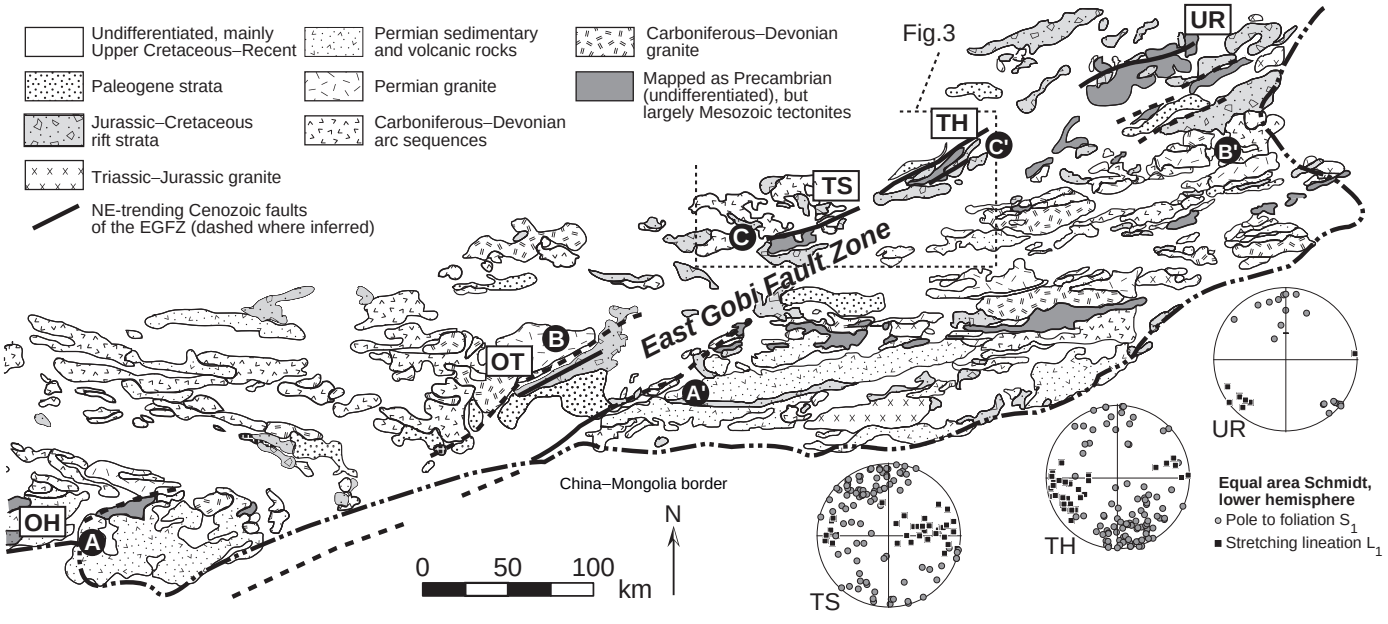

Fig. 2. Simplified geologic map of southeastern Mongolia modified after Tomurtogoo (1999). Abbreviations for localities discussed in the text are as follows: OH = Onch Hayrhan, OT = Oyu Tolgoi, TS = Tsagan Subarga, TH = Tavan Har; UR = Urgun. The map shows location of possible offset markers across the EGFZ (see text for discussion). A–A′ and B–B′ correspond to Paleozoic markers N–N′ and K–K′ from Fig. 2 of Lamb et al. (1999), and C–C′ represents Lower Cretaceous lacustrine units.

Please cite this article as: Webb, L.E., et al., Late Triassic sinistral shear in the East Gobi Fault Zone, Mongolia, Tectonophysics (2010), doi:10.1016/j.tecto.2010.09.033

kinematic lithologies that further bracket the timing of ductile sinistral shear in the East Gobi Fault Zone as Middle to Late Triassic.

2. Geology of the Tsagan Subarga and Tavan Har areas and evidence for early Mesozoic ductile sinistral shear

The tectonic framework of southeastern Mongolia is a vast accretionary complex involving Carboniferous–Devonian arc terranes of the Altaid tectonic collage (Sengor and Natal'in, 1996; Lamb and Badarch, 2001). The EGFZ follows the southern edge of the Altaid complex and runs immediately north of the Permian Tian Shan–Yin Shan suture zone and highly deformed and metamorphosed Lower–Upper Permian turbidite successions that mark final closure of a remnant ocean basin between the Paleozoic arc terranes and Tarim and the North China block (Johnson et al., 2008).

The Tsagan Subarga and Tavan Har areas (Figs. 2 and 3) are within the East Gobi Basin and represent basement block uplifts associated with Late Jurassic–Early Cretaceous rifting. The pre-Mesozoic units comprise variably metamorphosed Devonian–Carboniferous igneous and sedimentary sequences interpreted to represent a complex arc system (Lamb and Badarch, 2001; Badarch et al., 2002) and have suffered multiple generations of deformation. Structural and geochronologic data from the region are extremely limited and to date have primarily focused on the Paleozoic history of igneous activity and tectonism relevant to ore deposits in the region (e.g. Lamb and Cox, 1998; Watanabe and Stein, 2000; Perello et al., 2001). Evidence for regional Paleozoic greenschist-facies metamorphism and regional folding in the Devonian–Carboniferous units have been documented in the region north of the Tavan Har area (Blight et al., 2008). Higher grade metamorphic and igneous rocks within the Tsagan Subarga and Tavan Har blocks are still in some cases thought to represent Precambrian basement (e.g. Tomurtogoo, 1999).

The best exposures of the ductile shear zone are found in the northern Tavan Har basement block, part of a structural high between the Zuunbayan and Unegt subbasins that formed during Late Jurassic–Early Cretaceous rifting (Graham et al., 2001). There, the NE-striking shear zone fabrics and Mesozoic and Cenozoic block-bounding faults are apparent in satellite imagery (Fig. 4). The North Zuunbayan fault

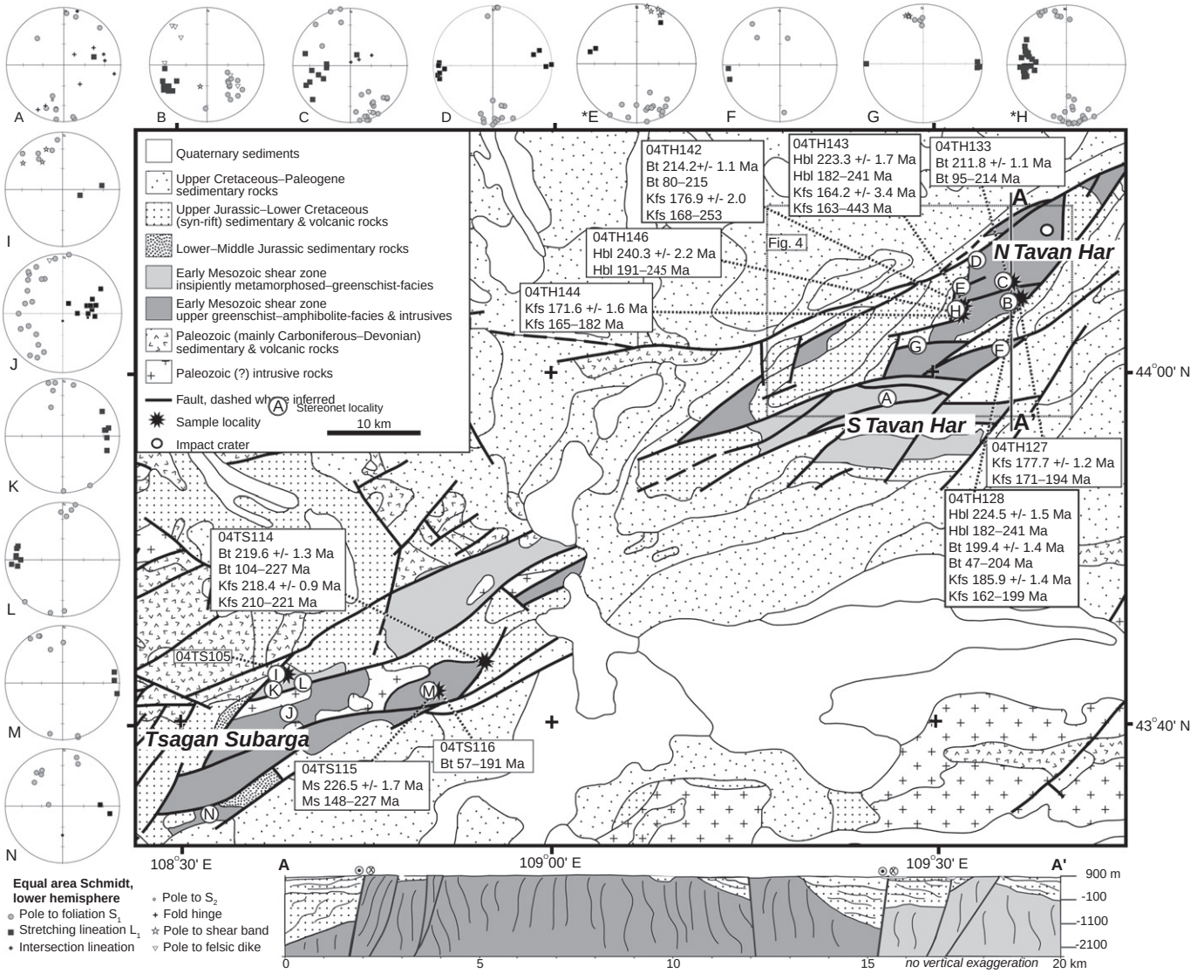

Fig. 3. Geologic map of the Tsagan Subarga and Tavan Har blocks of the East Gobi Fault Zone (based on the map of Borzakovskiy et al., 1982) showing distribution of new $^{40}Ar/^{39}Ar$ age data and localities discussed in text and Fig. 4. Structural data from the Tavan Har and Tsagan Subarga basement blocks are shown in equal area lower hemisphere Schmidt nets. Letters next to stereonets correspond to data collected in vicinity of lettered localities shown on the map. Asterisks indicate stereonets in which a subset of the data was published in Lamb et al. (1999).

Please cite this article as: Webb, L.E., et al., Late Triassic sinistral shear in the East Gobi Fault Zone, Mongolia, Tectonophysics (2010), doi:10.1016/j.tecto.2010.09.033

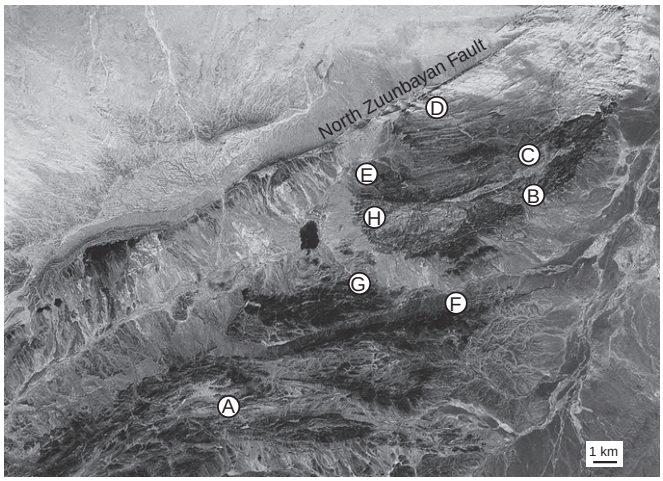

Fig. 4. Landsat image (https://zulu.ssc.nasa.gov/mrsid/) of the Tavan Har region. Location of area is indicated in Fig. 3. Stereonet data locations are shown as in Fig. 3 for reference.

runs along the northeastern margin of Tavan Har, roughly paralleling the shear zone, and has been active both in the Late Jurassic–Early as a normal fault and as a sinistral strike-slip fault in the Cenozoic (Johnson, 2004; Webb and Johnson, 2006). Rock types of northern Tavan Har include upper amphibolite-facies migmatites, amphibolite-facies mafic and felsic schists and gneisses, mylonitic shear zones, and apparent synkinematic intrusions. The latter are inferred based on magmatic fabrics which are concordant with that of the shear zone (e.g. at locality H, Fig. 3). Intermediate to felsic dikes cross-cut all rock types and are variably deformed. The shear zone is dominated by moderately–steeply-dipping NE-striking foliations and stretching lineations that plunge moderately–shallowly to the WSW or ENE (Fig. 3). Both a decrease in metamorphic grade and an overall increase in strain are apparent northward across the northern Tavan Har block, though discrete mylonitic shear zones are found cross-cutting the migmatites and gneisses near the southern margin. While there is some variability in foliation and lineation trends, no significant difference has been observed between the higher grade gneisses and mylonites (e.g. localities B and C (dominated by gneiss) and locality D (mylonites)). Kinematic indicators such as sigma and delta-type objects, asymmetric boudinage, and S–C fabrics indicate the ductile shear zone is dominated by sinistral shear sense (e.g. Fig. 5a). Mylonites have also been observed at southern Tavan Har where metamorphic grade is up to greenschist-facies (Fig. 3). The variability in metamorphic grade and orientation of structural fabrics between northern and southern Tavan Har is at least in part a result of their juxtaposition via Cenozoic strike-slip faulting (Webb and Johnson, 2006). Though the metamorphic basement in the region is generally in fault contact with Mesozoic strata, locally Lower Cretaceous strata onlap shear zone rocks on the western margin of northern Tavan Har (e.g. west of locality D, Figs. 3 and 4).

Lithologies and ductile deformation observed at Tsagan Subarga appear to correlate with that observed at Tavan Har. Transects conducted from north to south across Tsagan Subarga reveal a progressive increase in metamorphic grade from incipiently metamorphosed Carboniferous sedimentary and volcanic rocks into greenschist-facies and amphibolite-facies metasedimentary and metavolcanic lithologies. However we note that, as at Tavan Har, relationships are complicated due to multiple subsequent brittle deformation events. Variably metamorphosed Paleozoic volcanic and sedimentary sequences are caught up in discrete zones of mylonitic deformation whereas higher grade rocks are more pervasively deformed. Felsic intrusive units exhibiting both magmatic and solid state deformation were observed in southernmost Tsagan Subarga (north and west of locality M, Fig. 3). The majority of the metamorphic tectonites are inferred to have Paleozoic volcanic and sedimentary protoliths based on both field and petrographic observations (Fig. 5b, and c). Kinematic indicators observed at Tsagan Subarga (sigma and delta-type objects) are consistent with sinistral shear.

3. Analytical procedures

Samples from both Tsagan Subarga and Tavan Har were processed for $^{40}Ar/^{39}Ar$ thermochronologic analyses in order to constrain the timing of deformation associated with the ductile sinistral shear zone. $^{40}Ar/^{39}Ar$ analyses were performed at the Syracuse University Noble Gas Isotopic Research Laboratory. Following sample selection via petrographic analysis, high-purity mineral separates (>99%) were prepared by standard rock-crushing, mineral-separation, and hand-picking techniques. After a final acetone wash, mineral separates were wrapped individually in Cu foil and stacked with GA1550 biotite standard (98.79 Ma; Renne et al., 1998) used to monitor the neutron dose. Samples were vacuum sealed in a quartz tube and irradiated for seven hours in the CLICIT facility at the Oregon State University Radiation Center.

$^{40}Ar/^{39}Ar$ analyses of unknowns were achieved via double-vacuum resistance-furnace heating experiments. Gas was extracted during standard furnace dwell times of twelve minutes and was then exposed for ten minutes to hot and cold SAES ST-707 getters for purification. The purified gas was analyzed in a Micromass 5400 mass spectrometer utilizing an ion-counting electron multiplier. The mass spectrometer has a sensitivity of approximately 1.023×10^{-04} amps per Torr.

Sample and flux monitor data were corrected for blanks, mass discrimination, decay of ^{37}Ar and ^{39}Ar, neutron-induced interfering isotopes, and atmospheric argon. Mass discrimination was monitored by analyzing known aliquots of atmospheric argon for which $^{40}Ar/^{36}A_{atm}$ measured $=291.63\pm1.25$ (mean of most recent 94 analyses $\pm$ one standard deviation). Correction factors used to account for interfering nuclear reactions were determined by analyzing argon extracted from irradiated optical grade, fused CaF_2 and K-glass. Correction factors used to account for interfering nuclear reactions for the irradiated samples are: $(^{40}Ar/^{39}Ar)_K=2.11800\times10^{-02}\pm0.06260\times10^{-02}$, $(^{36}Ar/^{37}Ar)_{Ca}=2.41913\times10^{-04}\pm0.04278\times10^{-04}$, $(^{39}Ar/^{37}Ar)_{Ca}=9.10475\times10^{-04}\pm0.00612\times10^{-04}$. J factors for samples were calculated using a linear interpolation utilizing the sample position between flux monitor packets in the irradiation tube. All ages were calculated using the decay constants recommended by Steiger and Jäger (1977). Age calculations for inverse isochron and apparent age data were achieved utilizing the program Isoplot 3.0 and error correlation coefficients were calculated based on methods discussed in Ludwig (2003).

Plateau ages are reported when the plateau criteria are met (see McDougall and Harrison, 1999); otherwise, weighted mean ages are reported if plateau-like segments exist. Errors on plateau and weighted mean ages are quoted at the 2σ level and include precision error in measurement of the irradiation parameter, J, for flux monitor GA1550 biotite. Analytical results are summarized in Table 1 and detailed sample data can be found in the data repository. Apparent age spectra for all samples are shown in Fig. 6. Inverse isochron ages, when defined, for amphibole, biotite, and muscovite are concordant with quoted plateau and weighted mean ages. Multi diffusion domain experiments were run on K-feldspar separates, however none of the samples yielded data amenable to modeling.

4. Sample descriptions and $^{40}Ar/^{39}Ar$ apparent ages

4.1. Tavan Har

Sample 04TH146 comes from banded migmatite gneiss with ptygmatic folds (Fig. 5d). No lineation was observed at the sample locality and foliations are variable and in some cases oblique to that of the shear zone. An amphibole mineral separate from the melanosome

Please cite this article as: Webb, L.E., et al., Late Triassic sinistral shear in the East Gobi Fault Zone, Mongolia, Tectonophysics (2010), doi:10.1016/j.tecto.2010.09.033

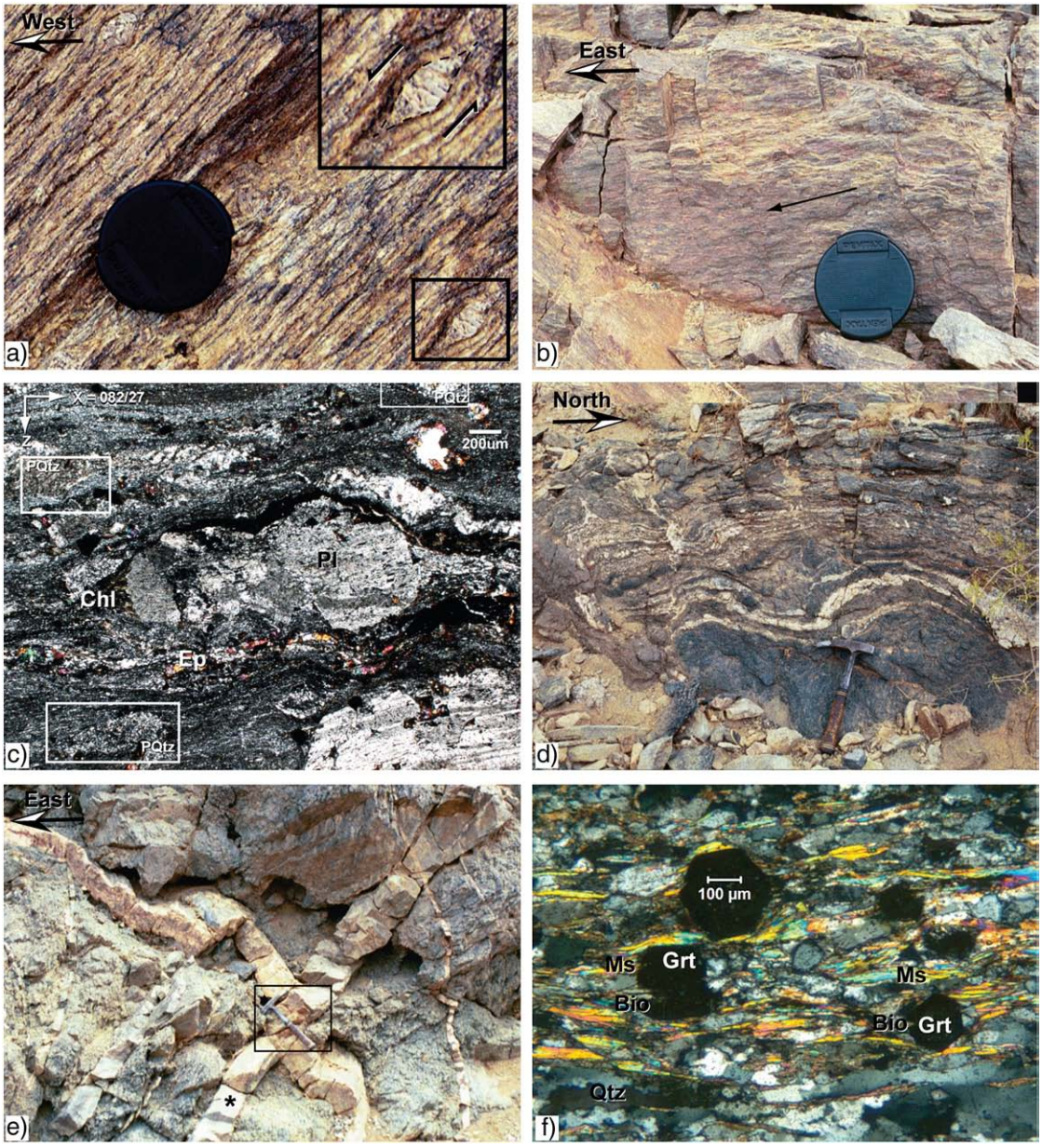

Fig. 5. Field photographs and sample photomicrographs. a) Augen gneiss at Tavan Har with sigma-type potassium feldspar porphyroclasts indicating sinistral shear sense. Photo locality is between sample localities for 04TH133 and 04TH128 on map in Fig. 3. b) Greenschist-facies mylonite zone in Paleozoic sedimentary and volcanic rocks at Tsagan Subarga. Arrow indicates plunge of lineation (foliation dip azimuth/dip angle = 168/70; lineation trend/plunge = 082/27). Lens cap for scale (diameter = 50 mm). Photomicrograph of sample 04TS105 taken from this outcrop is shown in panel c and the location of outcrop is shown in Fig. 3. c) Photomicrograph of sample 04TS105 taken from outcrop shown in panel b. Plagioclase porphyroclasts have chlorite tails and locally are cut by microfaults. Polycrystalline quartz fragments (PQtz) are abundant in the sample, which is interpreted to have a volcaniclastic protolith. Arrows in the upper left corner indicate orientation of thin section, cut parallel to finite lineation (X) and normal to finite foliation (Z); see panel b caption for orientation information. d) Field photograph of migmatite unit from which sample 04TH146 was taken. e) Field photo of sample 04TH127 locality. Box highlights hammer for scale; asterisk indicates dike that was sampled. f) Photomicrograph of sample 04TS115 (see discussion in text).

was analyzed. Microscopic evidence for deformation was mainly restricted to late stage brittle fractures with the exception of minor deformation twins and evidence for grain boundary migration in plagioclase. The sample yielded an apparent age spectrum with an argon loss profile with a minimum age ca. 191 Ma that ramped up to a plateau-like segment comprising 92.2% or the ^{39}Ar released with a weighted mean age of 240.3 ± 2.2 Ma.

Sample 04TH128 is garnet-bearing amphibolite-facies gneiss in which amphibole defines the stretching lineation. At outcrop scale, asymmetric boudinage of leucocratic veins within the sample indicate sinistral shear sense. Plagioclase displays deformation twins and is locally found as mantled porphyroclasts and quartz fabrics are characteristic of dynamic recrystallization via subgrain rotation; myrmekite is abundant. Amphibole boudinage are formed by synthetic shear bands and biotite appears to have grown at the expense of amphibole after deformation ceased. A late, brittle overprint is apparent at both outcrop and thin-section scale. Amphibole, biotite, and K-feldspar separates were analyzed. Amphibole yielded an argon loss profile with a minimum age of 183 Ma and plateau age of 224.5 ± 1.5 Ma. The biotite separate yielded a more extreme Ar-loss profile with minimum age of 47 Ma and a weighted mean age of 199.4 ± 1.4 Ma. The apparent age spectrum for K-feldspar yielded minimum and maximum ages of 162 and 199 Ma, respectively.

Sample 04TH143 comes from granite that locally displays magmatic fabrics concordant with that of the shear zone. The sample came from near an intrusive contact with foliated amphibolite. Fabric

Please cite this article as: Webb, L.E., et al., Late Triassic sinistral shear in the East Gobi Fault Zone, Mongolia, Tectonophysics (2010), doi:10.1016/j.tecto.2010.09.033

Table 1
Summary of $^{40}Ar/^{39}Ar$ results.

Sample	Description	Latitude °N	Longitude °E	Phase dated	Mass (mg)	Min age	Max age[a]	PA[b] (Ma)	WMA[c] (Ma)	2σ error (Ma)	%^{39}Ar	MSWD[d]
04TH146	Migmatite	44.054163	109.535455	Hbl	4.1	191	245		240.3	2.2	92.2	2.4
04TH128	Gneiss	44.068919	109.613452	Hbl	4.0	183	227	224.5		1.5	89.8	1.9
				Bt	1.0	47	204		199.4	1.4	60.9	3.1
				Kfs	1.8	162	199					
04TH143	Syn-kinematic intrusion	44.062667	109.537314	Hbl	5.9	182	241	223.3		1.7	95.6	1.02
				Kfs	1.8	163	443					
04TH142	Late syn- to post-kinematic dike	44.062667	109.537314	Bt	0.6	80	215	214.2		1.1	75.1	0.26
				Kfs	2.0	168	253					
04TH133	Intermediate dike	44.078931	109.604994	Bt	1.8	95	214	211.8		1.1	86.2	0.65
04TH127	X-cutting dike	44.068919	109.613452	Kfs	1.4	171	194					
04TH144	Pegmatite	44.054163	109.535455	Kfs	1.7	165	182					
04TS115	Garnet-grade metapelite	43.697276	108.846791	Ms	0.3	148	227	226.5		1.7	88.9	0.25
04TS116	Garnet-grade metapelite	43.697276	108.846791	Bt	0.6	57	191					
04TS114	Deformed granite	43.722820	108.918174	Bt	0.6	104	227	219.6		1.3	77.7	1.09
				Kfs	1.3	210	221	218.4		0.9	86.4	1.3

[a] Maximum ages are subjective (e.g., do not include anomalously old ages in lowest temperature steps.).
[b] PA = plateau age.
[c] WMA = weighted mean age.
[d] MSWD = mean square weighted deviates.

in the granite is best described as seriate-interlobate. Brittle fractures are present in thin section and quartz grains show undulatory extinction. Step-heating of an amphibole separate from the granite yielded a loss profile with a minimum age of 182 Ma and a plateau age of 223.3 ± 1.7 Ma. K-feldspar yielded minimum and maximum apparent ages of 163 and 443 Ma, respectively.

Sample 04TH142 comes from a late stage pegmatite dike intruded parallel to the foliation in biotite-rich, intermediate composition mylonites. Biotite grains are decussate (interlocking), feldspars show deformation twins, and quartz recrystallization was facilitated by a combination of subgrain rotation and grain boundary migration; myrmekite is relatively abundant. Late brittle fractures are filled with hematite and undulatory extinction in quartz is also evident. A biotite separate from the pegmatite yielded an argon loss profile with a minimum apparent age of 80 Ma and a plateau age of 214.2 ± 1.1 Ma. K-feldspar yielded minimum and maximum apparent ages of 168 and 253 Ma, respectively.

Sample 04TH133 is from a dike with intermediate (~andesitic) composition and porphyritic texture and was inferred to be a hypabyssal volcanic dike in the field. The orientation of the dike (337/77) is roughly concordant with that of the shear zone where sampled, but is observed in Google Earth imagery to cross-cut the foliation and extend a total of at least 0.5 km in the WNW–ESE orientation. Any offsets of the dike in the observable extent are limited to <10 m. Exposure at this locality was not continuous but units exposed on either side of the dike included quartzo-feldspathic gneiss and mylonite. The fabric is seriate with quartz grains forming the finest grain size population and plagioclase defining the largest; plagioclase grains are rectangular and preserve magmatic zoning. Quartz grain shapes suggest that grain boundary area reduction recovery processes were active. Biotite is decussate. Step-heating of biotite yielded an argon loss profile with minimum apparent age of 95 Ma and a plateau age of 211.8 ± 1.1 Ma.

Sample 04TH127 is from pegmatite dike that cross-cuts gneissic rocks of the shear zone (Fig. 4E; proximal to location for 04TH128). The dike appears relatively undeformed in outcrop and is characterized by granophyric textures in thin section. Myrmekite is present, as well as deformation twins in feldspar. Hematite fills late stage fractures. K-feldspar yielded an apparent age spectrum with minimum and maximum ages of 171 and 194 Ma, respectively.

Sample 04TH144 is a pegmatite sample collected near the locality of sample 04TH146. Feldspars in this sample exhibit core–mantle structures; quartz indicates recrystallization via a combination of subgrain rotation and grain boundary migration. Late stage fractures are filled with hematite. Step-heating of K-feldspar yielded minimum and maximum apparent ages of 165 and 182 Ma, respectively.

4.2. Tsagan Subarga

Sample 04TS115 is a garnet-grade metapelite. Kinematic indicators for sinistral shear sense were observed within the larger outcrop of NE-striking metamorphic tectonites. Garnet porphyroclasts preserve evidence for once having of euhedral crystal shapes; embayments on otherwise equant garnet grains formed as a result of growth of white mica and biotite as wings during deformation (Fig. 5f), though no kinematic interpretation is possible from this particular sample. Garnet cores are full of microcrystalline inclusions while rims appear inclusion-free. Deformation is interpreted to have accompanied retrograde metamorphism. Quartz microstructures record evidence for grain boundary migration and subgrain rotation; the higher temperature quartz fabrics are overprinted by undulatory extinction and deformation bands. Step-heating of muscovite yielded an argon loss profile with a minimum apparent age of 148 Ma and a plateau age of 226.5 ± 1.7 Ma.

Sample 04TS116 is garnet-bearing schist. Biotite grew at the expense of garnet during deformation and locally exhibits alteration to chlorite. Quartz exhibits evidence for both grain boundary migration and undulatory extinction. Late stage fractures are filled with hematite. Step-heating of biotite from this sample yielded an apparent age spectrum with an argon loss profile and gave minimum and maximum ages of 57 and 191 Ma, respectively.

Sample 04TS114 is from granite in fault contact with Upper Jurassic sedimentary rocks. The granite records evidence for ductile deformation prior to the cataclastic deformation overprint associated with the fault contact. Ductile deformation was accommodated by dynamic recrystallization of quartz via subgrain rotation; feldspars exhibit deformation twins. Biotite yielded an argon loss profile with a minimum age of 104 Ma and a plateau of 219.6 ± 1.3 Ma. K-feldspar yielded minimum and maximum ages of 210 and 221 Ma, respectively.

5. Discussion

5.1. Timing of deformation

The oldest $^{40}Ar/^{39}Ar$ age from the metamorphic rocks, 240.3 ± 2.2 Ma (early Middle Triassic/Anisian), was obtained on amphibole from a migmatite (04TH146) and is interpreted to provide a minimum age for a partial melting event. Because foliation in the sample and other observed

Please cite this article as: Webb, L.E., et al., Late Triassic sinistral shear in the East Gobi Fault Zone, Mongolia, Tectonophysics (2010), doi:10.1016/j.tecto.2010.09.033

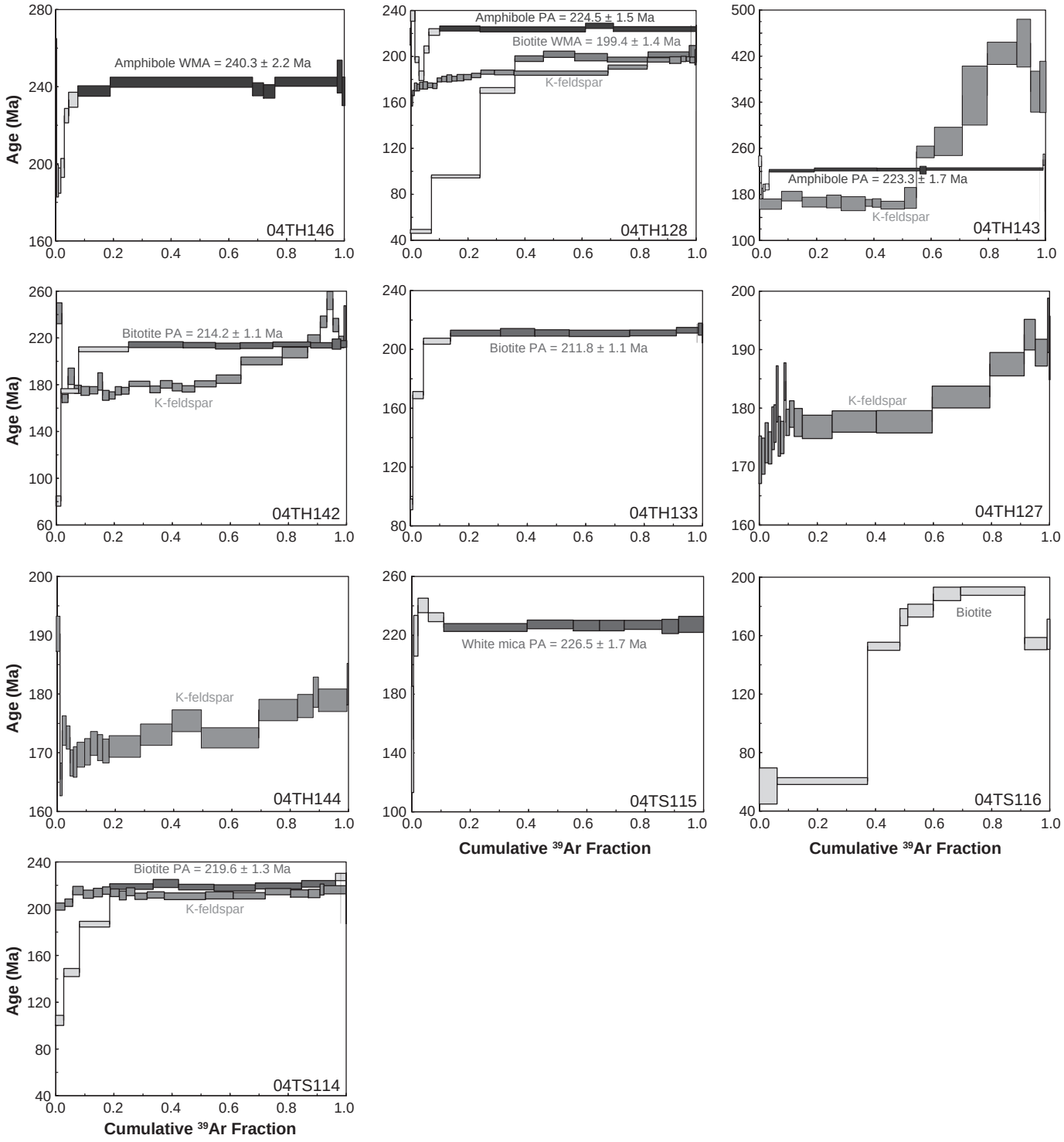

Fig. 6. Compiled apparent $^{40}Ar/^{39}Ar$ age spectra. Box heights and quoted errors are 2σ. Darker boxes in an apparent age spectrum are those used in plateau age (PA) or weighted mean age (WMA) calculations.

migmatite lithologies is principally defined by compositional banding and few if any lineations are apparent, partial melting may have occurred prior to activation of the shear zone. U/Pb zircon dating of migmatites, gneisses, and mylonites at Tavan Har is the topic of ongoing investigation to constrain the relationship between partial melting and ductile sinistral shear.

The timing of deformation associated with cooling through amphibolite to upper greenschist-facies conditions is best constrained to have occurred by ca. 225 Ma (early Late Triassic/Carnian) by $^{40}Ar/^{39}Ar$ dating of amphibole that defines the stretching lineation in amphibolite-facies gneiss (04TH128; 224.5 ± 1.5 Ma). Similar ages were obtained for synkinematic white mica growing as tails on garnet in garnet-grade metapelite (04TS115; 226.5 ± 1.4 Ma), and amphibole from a synkinematic intrusion (04TH143; 223.3 ± 1.7 Ma). This segment of the temperature–time–deformation path is inferred by integrating the thermochronologic constraints with microstructures. For example, sample 04TH128 (amphibolite gneiss) records microstructures consistent with deformation during retrograde metamorphism from amphibolite–upper greenschist-facies conditions. From higher to lower temperature (assuming average strain rates), relevant

Please cite this article as: Webb, L.E., et al., Late Triassic sinistral shear in the East Gobi Fault Zone, Mongolia, Tectonophysics (2010), doi:10.1016/j.tecto.2010.09.033

microstructural observations include abundant myrmekite, feldspars with core–mantle structures, dynamic recrystallization of quartz via subgrain rotation (see Passchier and Trouw, 2005, and references therein). Because of this record for a continuum of deformation through ~650–450 °C and an overlapping range in possible closure temperatures for amphibole from ~600 to 470 °C depending on cooling rate (Reiners and Brandon, 2006), we infer that the $^{40}Ar/^{39}Ar$ plateau age of 224.5 ± 1.5 Ma provides a good estimate for the timing of deformation at amphibolite–upper greenschist-facies conditions. The growth of biotite post-deformation and the preservation of subgrain rotation microstructures in quartz (as opposed to foam textures associated with recovery) in this same sample are best reconciled with static biotite growth at relatively low temperatures. The $^{40}Ar/^{39}Ar$ biotite weighted mean age of 199.4 ± 1.4 Ma from this sample is interpreted as a minimum age for cessation of deformation.

Waning of distributed shear zone activity, at least locally, is partially constrained by a 211.8 ± 1.1 Ma $^{40}Ar/^{39}Ar$ age obtained on biotite from a dike that cross-cuts the foliation (04TH133). The integrated field, satellite imagery, and microstructural data indicate fairly rapid cooling during crystallization, little or no offset, and only minor ductile deformation at the microscopic scale. The biotite age obtained for this sample is concordant to the 209 ± 4 Ma (2σ) $^{40}Ar/^{39}Ar$ weighted mean biotite age (calculated for ~90% of the ^{39}Ar released) obtained reported by Lamb et al. (1999) for synkinematic biotite from an S–C mylonite (near locality E, Fig. 3). The combined data suggest that broadly distributed deformation had ceased by this time and strain was likely focused in more discrete mylonite zones.

All apparent age spectra, including the biotite analyzed by Lamb et al. (1999), are complicated by argon loss profiles. In the case of all hydrous phases that were analyzed (i.e. amphibole, white mica, and biotite), minimum apparent ages appear to be related to Mesozoic and Cenozoic brittle deformation overprints based on geologic context and microstructural evidence; minimum ages range from 191 to 47 Ma. These loss profiles likely relate to the fact the mineral phases experienced either enhanced diffusive loss due to grain size reduction and/or neocrystallization during deformation (e.g. Dunlap and Kronenberg, 2001). Hydrothermal fluids associated with regional volcanic activity during Late Jurassic–Early Cretaceous rifting (Graham et al., 2001) or Cenozoic faulting (Webb and Johnson, 2006) may also have an influence. The fact that the youngest minimum ages all come from biotite samples may imply that this phase is particularly susceptible to one or all of these processes during late stage deformation events.

Despite the fact that data acquired from $^{40}Ar/^{39}Ar$ step-heating experiments on K-feldspar samples could not be modeled to obtain thermal histories, the data do provide useful information. There is a distinct difference in the range of ages obtained from lower temperature steps from samples from the Tavan Har block compared to the sample from Tsagan Subarga (Fig. 6). Tavan Har K-feldspar minimum ages comprise a cluster ranging from ~171 to 162 Ma and the majority ages obtained over the course of the step-heating experiments are younger than 190 Ma. The data thus imply relatively slow cooling below ~300 °C in the Early Jurassic following shearing at amphibolite–upper greenschist-facies conditions ca. 225 Ma, and are consistent with final cooling below ~150 °C in the Middle Jurassic constrained by apatite fission track data (Taylor et al., 2008). Conversely, sample 04TS114 K-feldspar produced a fairly flat apparent age spectrum yielding a plateau age of 218.4 ± 0.9 Ma. Biotite from this same sample yielded a plateau age of 219.6 ± 1.3 Ma and thus these data imply relatively rapid cooling in the Late Triassic following shearing at amphibolites-facies conditions. The approximate cooling rates attending shear zone activity are ~40 °C Myr^{-1} and ~20 °C Myr^{-1} for the Tsagan Subarga and Tavan Har blocks, respectively (Fig. 7). The K-feldspar data are interpreted here to reflect the fact that deeper structural levels of the Early Mesozoic shear zone are likely presently exposed at Tavan Har compared to Tsagan Subarga. Interpretations of depth to basement in seismic reflection profiles indicate that the Late Jurassic–Early Cretaceous Zuunbayan rift basin deepens to the northeast (Johnson, 2004). Differential throw on the basin bounding faults along strike is consistent with exhumation of deeper structural levels of the shear zone at Tavan Har compared to Tsagan Subarga during Late Jurassic–Early Cretaceous rift basin formation. The apparent divergence in Late Triassic thermal histories shown in Fig. 7 can be linked to deformation and differential exhumation subsequent to the Late Triassic and does not require primary differences between the Late Triassic histories of the two basement blocks.

5.2. Tectonic implications

The available data argue for a Late Triassic ductile sinistral shear zone within the EGFZ. The ductile shear zone activity post dates the

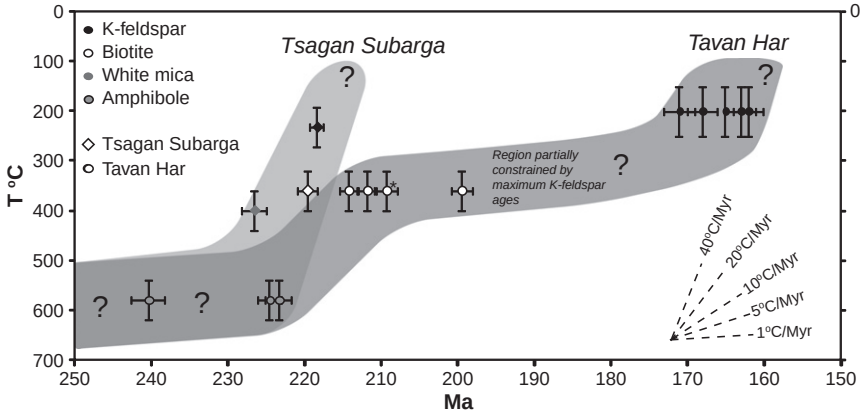

Fig. 7. Proposed thermal histories of the Tsagan Subarga and Tavan Har blocks of the East Gobi Fault Zone. Data for mineral phases are color coded; samples from Tavan Har are denoted by circles and Tsagan Subarga by diamonds. Only minimum K-feldspar ages are plotted (see Table 1). The asterisk denotes biotite age reported by Lamb et al. (1999). Closure temperatures were estimated from Reiners and Brandon (2006) assuming cooling rates in the range of 10–100 °C Myr^{-1} and are plotted using the following values: T_c amphibole = 580 ± 40 °C, T_c white mica = 400 +/− 40 °C, and T_c biotite = 360 +/− 40 °C. Due to apparent slow cooling, K-feldspar minimum ages from Tavan Har are approximated to correspond to cooling through 200 +/− 50 °C, whereas 230 +/− 40 °C is used for minimum K-feldspar ages from Tsagan Subarga due to apparent rapid cooling. The offset in apparent ages from different thermochronometers has a larger impact on apparent cooling rates here than choice of closure temperature. Readers are referred to McDougall and Harrison (1999) and Reiners and Brandon (2006) for discussion on closure temperatures. The deviation in thermal histories for Tavan Har and Tsagan Subarga may reflect that different structural levels are presently exposed at the surface which is controlled in part by the Late Jurassic–Early Cretaceous rift history.

Please cite this article as: Webb, L.E., et al., Late Triassic sinistral shear in the East Gobi Fault Zone, Mongolia, Tectonophysics (2010), doi:10.1016/j.tecto.2010.09.033

Permian Tian Shan–Yin Shan suture zone and thus occurred in an intracontinental setting. The argon data suggest rapid cooling in the Late Triassic (~40–20 °C Myr^{-1}) accompanied deformation, a result not predicted for pure strike-slip deformation. Rapid cooling requires an additional mechanism for exhumation and cooling; possibilities include: 1) sinistral shear was associated with transtension and coeval ductile thinning or tectonic denudation; or, 2) sinistral shear was associated with transpression and coeval erosional denudation (Ring et al., 1999). A third possibility is that the Late Triassic fabrics have been rotated into the present orientation by subsequent deformation events. Discerning between these possibilities is part of our ongoing research, but transtension appears to be most consistent with the current data. Middle to Upper Triassic strata (predicted for erosional denudation associated with transpression) are notably absent in the region, whereas lineation and foliation pairs observed in the sinistral shear zone are most consistent with a transtensional dip-slip component.

Exposures of the ductile Late Triassic shear in the EGFZ have been traced at least 100 km to the NE of Tavan Har in the Urgun area (Fig. 2), the continuation beyond which is uncertain. To the southwest, the surficial expression of ductile shear locally dies out at western margin of the Tsagan Subarga block, however the shear zone plots along the southern margin of a linear magnetic high (Maus, 2009) that continues southwest from Tsagan Subarga toward the Chinese border. Final exhumation and thus the surficial exposure of the shear zone are likely controlled by the Late Jurassic–Early Cretaceous fault block geometry and subsequent Cenozoic strike-slip faulting (Webb and Johnson, 2006). Constraining offset along the EGFZ is part of ongoing research, but given initial estimates of displacement associated with the Late Triassic phase of sinistral ductile shear (~250–100 km; Lamb et al., 1999; Heumann et al., 2008) it is quite possible that the shear zone extended hundreds of km farther in either direction (cf. Kim and Sanderson, 2005). Wang et al. (2005) suggest Triassic movement on the Altyn Tagh fault around 250–230 Ma, based on argon dating of sinistral mylonites in the eastern Kunlun Shan. The possibility of a long-lived connection between the EGFZ and the Altyn Tagh fault is intriguing and seems possible in light of these data, although piercing point studies do not support major pre-Jurassic movement on the Altyn Tagh fault (Ritts and Biffi, 2000).

In southernmost Mongolia along the Chinese border, Johnson et al. (2001) documented ductile fabrics recording NE–SW extension that are overprinted by the Early Cretaceous Yagan-Onch Hayrhan metamorphic core complex (Fig. 1). Wang et al. (2004) reported a 228 ± 7 Ma U/Pb zircon age from mylonitic biotite-quartz monzonites from the core complex on the Chinese side of the border, interpreted to date the timing of intrusion of a suite of Late Triassic plutons in a post-collisional or post-orogenic extensional setting. Thus, the NE–SW extensional deformation recorded by Johnson et al. (2001) may be Late Triassic in age. Late Triassic extension has been proposed and documented elsewhere in proximity to the Permian Yin Shan suture zone. Lamb et al. (2008) reported Late Triassic K-feldspar cooling ages from red akali granites in the Shin Jinst area interpreted to represent cooling of late stage collisional granites or granites emplaced during post-orogenic uplift and collapse. A metamorphic core complex in the Sonid Zuoqi area ~300 km east–southeast of Tavan Har represents high strain, NNE–SSW extension in the Late Triassic along a low angle detachment fault (Fig. 1; Davis et al., 2004). Late Triassic intraplate E–W extension associated with N–NE-striking normal faults has also been noted in northwest Ordos in Inner Mongolia (Ritts et al., 2009).

5.3. Potential drivers of deformation in the EGFZ

To the north of the EGFZ, the narrow Mongol-Okhotsk ocean between Mongolia and the Siberian block was closing from west to east, associated with subduction beneath Mongolia, by the early Mesozoic. Paleomagnetic data are complicated by overprinting but generally imply continued closure near the Pacific margin through at least the Early Cretaceous (e.g., Xu et al., 1997; Halim et al., 1998; Kravchinsky et al., 2002). Conflicting estimates for the timing of the main collisional event in the vicinity of northern Mongolia, both of which based on geologic mapping and ages of marine–non-marine stratigraphic transitions, include Early Triassic (Zonenshain et al., 1990) or the Middle–Late Jurassic boundary (Zorin, 1999). A combined Mongolia–North China block may still have been moving north relative to Siberia in the Triassic, albeit slowly, at the time that sinistral ductile shear zones were active in the EGFZ. To the south of the EGFZ, the Triassic was associated with closure of the Paleotethys and interactions between the Qiangtang and Kunlun blocks and the North and South China blocks (e.g., Dewey et al., 1988; Hacker et al., 2000; Kapp et al., 2000; Roger et al., 2008).

Late Triassic shear in the EGFZ is likely the result of far field forces associated with coeval convergent boundaries in Asia, and is consistent with existing paleotectonic reconstructions (e.g. Natal'in and Sengor, 2005). Collisions associated with closure of the Paleotethys and/or closure of the Mongol-Okhotsk resulted in reactivation of favorably-oriented inherited crustal structures within the North China–Mongolia continental interior. Deformation was associated with NE–SW to E–W extension and focused in a zone of relatively weak and heterogeneous crust within recently collided arc systems, essentially sandwiched between Precambrian blocks to the north (Siberian craton) and the south (North China Block). An additional possibility linking Late Triassic shear in the EGFZ with core complex formation in northern China includes oblique transtension associated with collapse of the Late Permian suture zone between the Altaids and the North China craton in this area (Johnson et al., 2008).

6. Conclusions

Metamorphic tectonites of the Tsagan Subarga and Tavan Har blocks, previously mapped as Precambrian basement, comprise a shear zone dominated by steeply-dipping, northeast-striking sinistral shear zone that can be traced for ~250 km along strike. Field and petrographic analyses indicate that the protoliths of the metamorphic tectonites are Paleozoic arc igneous and sedimentary sequences, and bring into question the existence of Precambrian basement in the region. $^{40}Ar/^{39}Ar$ step-heating analyses of minerals from pre-, syn-, and late- to post-kinematic lithologies indicate that ductile sinistral shear in the EGFZ post dates an Early Triassic or older partial melting event. The main phase of deformation associated with cooling through amphibolite-facies to upper greenschist-facies conditions occurred at 225 Ma and appears to have waned by 210 Ma. Cooling rates inferred from the $^{40}Ar/^{39}Ar$ data are on the order of 40–20 °C Myr^{-1} during shear zone activity. Relatively rapid Late Triassic cooling suggests a transtensional component to the deformation and is coincident with core complex formation in northern China. Late Triassic intraplate deformation in the EGFZ correlates temporally with closure of the Paleotethys and Mongol-Okhotsk oceans and thus likely represents reactivation of a primary lithospheric structure by far field stresses associated with plate boundary processes, representing an early Mesozoic analog for Cenozoic intraplate deformation associated with the India–Asia collision.

Acknowledgements

This work was supported by the National Science Foundation grant numbers EAR-0537165 and EAR-0929902 to L. Webb, and EAR-0537318 to C. Johnson. The research also benefited from American Chemical Society, Petroleum Research Fund grant 40193-G8 to C.L. Johnson. We thank M. Affolter, N. Manchuk, and G. Sersmaa for their assistance in the field. Willis Hames and an anonymous reviewer are thanked for thoughtful reviews that improved the manuscript.

Please cite this article as: Webb, L.E., et al., Late Triassic sinistral shear in the East Gobi Fault Zone, Mongolia, Tectonophysics (2010), doi:10.1016/j.tecto.2010.09.033

Appendix A. Supplementary data

Supplementary data to this article can be found online at doi:10.1016/j.tecto.2010.09.033.

References

Badarch, G., Cunningham, W.D., Windley, B.F., 2002. A new terrane subdivision for Mongolia; implications for the Phanerozoic crustal growth of Central Asia. Journal of Asian Earth Sciences 21, 87–110.

Blight, J.H.S., Cunningham, D., Petterson, M.G., 2008. Crustal evolution of the Saykhandulaan Inlier, Mongolia: implications for Palaeozoic arc magmatism, polyphase deformation and terrane accretion in the Southeast Gobi Mineral Belt. Journal of Asian Earth Sciences 32, 142–164.

Borzakovskiy, U.A., Suetenko, O.D., Gluhovskaja, N.B., Golovchenko, E.E., Kandinov, M. N., Potapov, A.V., 1982. Geological Map of the South Gobi. Ministry of Geology of the USSR, Moscow.

Davis, G.A., Xu, B., Zheng, Y.D., Zhang, W.J., 2004. The Sonid Zuoqi metamorphic core complex, Inner Mongolia, China. Earth Science Frontiers 11, 134–144.

Dewey, J.F., Schackleton, R.M., Chengfa, C., Yiyin, S., 1988. The Geological Evolution of Tibet: Report of the 1985 Royal Society — Academia Sinica Geotraverse of Qinghai–Xizang Plateau. Philosophical Transactions of the Royal Society of London Series A, Mathematical and Physical Sciences 327, 379–413.

Dunlap, W.J., Kronenberg, A.K., 2001. Argon loss during deformation of micas: constraints from laboratory deformation experiments. Contributions to Mineralogy and Petrology 141 (2), 174–185.

Graham, S.A., Hendrix, M.S., Johnson, C.L., Badamgarav, D., Badarch, G., Amory, J., Porter, M., Barsbold, R., Webb, L.E., Hacker, B.R., 2001. Sedimentary record and tectonic implications of late Mesozoic rifting, southeast Mongolia. Geological Society of America Bulletin 113, 1560–1579.

Hacker, B.R., Ratschbacher, L., Webb, L.E., McWilliams, M., Calvert, A., Dong, S., Wenk, H.-R., Chateigner, D., 2000. Exhumation of the ultrahigh-pressure continental crust in east-central China: Cretaceous and Cenozoic unroofing and the Tan-Lu Fault. Journal of Geophysical Research 105, 13303–13338.

Halim, N., Kravchinsky, V., Gilder, S., Cogne, J.-P., Alexyutin, M., Sorokin, A., Courtillot, V., Chen, Y., 1998. A palaeomagnetic study from the Mongol-Okhotsk region: rotated Early Cretaceous volcanic and remagnetized Mesozoic sediments. Earth and Planetary Science Letters 159, 133–145.

Heumann, M., Johnson, C., Webb, L., Taylor, J., 2008. Detrital zircon and sandstone provenance analysis from Permian and Lower Cretaceous sedimentary units to constrain total and incremental left-lateral offset along the East Gobi Fault Zone, southeastern Mongolia. 2008 Fall Meeting Supplemental Abstracts: Eos Transactions, AGU. TE43-01.

Houseman, G., England, P., 1993. A lithospheric-thickening model for the Indo–Asian collision. In: Yin, A., Harrison, M. (Eds.), The Tectonic Evolution of Asia. Cambridge University Press, Cambridge, pp. 3–17.

Jahn, B., 1999. Introduction to IGCP-420; continental growth in the Phanerozoic; evidence from the Central Asian orogenic belt (CAOB). Memoires de Geosciences Rennes, Special Issue 2, 1–5.

Johnson, C.L., 2004. Polyphase evolution of the East Gobi basin: sedimentary and structural records of Mesozoic–Cenozoic intraplate deformation in Mongolia. Basin Research 16, 79–99.

Johnson, C.L., Webb, L.E., Graham, S.A., Hendrix, M.A., Badarch, G., 2001. Sedimentary and structural records of late Mesozoic high-strain extension and strain partitioning, East Gobi basin, southern Mongolia. In: Hendrix, M.S., Davis, G.A. (Eds.), Paleozoic and Mesozoic Tectonic Evolution of Central and Eastern Asia: From Continental Assembly to Intracontinental Deformation: Geological Society of America Memoir, pp. 413–434.

Johnson, C.L., Amory, J., Zinniker, D., Lamb, M.A., Graham, S.A., Affolter, M., Badarch, G., 2008. Sedimentary response to arc-continent collision, Permian, southern Mongolia. In: Draut, A., Clift, P., Scholl, D. (Eds.), Formation and Applications of the Sedimentary Record in Arc Collision Zones. Geological Society of America, pp. 363–390.

Kapp, P., Yin, A., Manning, C.E., Murphy, M., Harrison, T.M., Spurlin, M., Lin, D., Xi-Guang, D., Cun-Ming, W., 2000. Blueschist-bearing metamorphic core complexes in the Qiangtang block reveal deep crustal structure of northern Tibet. Geology 28, 19–22.

Kim, Y.-S., Sanderson, D.J., 2005. The relationship between displacement and length of faults: a review. Earth-Science Reviews 68, 317–334.

Kravchinsky, V.A., Sorokin, A.A., Courtillot, V., 2002. Paleomagentism of Paleozoic and Mesozoic sediments from the southern margin of Mongol-Okhotsk ocean, far eastern Russia. Journal of Geophysical Research 107. doi:10.1029/2001JB000672.

Lamb, M.A., Badarch, G., 2001. Paleozoic sedimentary basins and volcanic arc systems of southern Mongolia: new geochemical and petrographic constraints. In: Hendrix, M. S., Davis, G.A. (Eds.), Paleozoic and Mesozoic Tectonic Evolution of Central and Eastern Asia: From Continental Assembly to Intracontinental Deformation. Geological Society of America, pp. 117–149.

Lamb, M.A., Cox, D., 1998. New $^{40}Ar/^{39}Ar$ age data and implications for porphyry copper deposits of Mongolia. Economic Geology 93, 524–529.

Lamb, M.A., Hanson, A.D., Graham, S.A., Badarch, G., Webb, L.E., 1999. Left-lateral sense offset of upper Proterozoic to Paleozoic features across the Gobi Onon, Tost, and Zuunbayan faults in southern Mongolia and implications for other Central Asian faults. Earth and Planetary Science Letters 173, 183–194.

Lamb, M.A., Badarch, G., Navratil, T., Poier, R., 2008. Structural and geochronologic data from the Shin Jinst area, eastern Gobi Altai, Mongolia: implications for Phanerozoic intracontinental deformation in Asia. Tectonophysics 451, 312–330.

Ludwig, K.R., 2003. Isoplot/EX, rev. 3.00, a Geochronological Toolkit for Microsoft Excel. Berkeley Geochronology Center Special Publication, 4. 71 pp.

Maus, S.A.O., 2009. EMAG2: a 2-arc min resolution Earth Magnetic Anomaly Grid compiled from satellite, airborne, and marine magnetic measurements. Geochemistry Geophysics Geosystems 10. doi:10.1029/2009GC002471.

McDougall, I., Harrison, T.M., 1999. Geochronology and Thermochronology by the 40Ar/39Ar Method. Oxford University Press, Oxford. 269 pp.

Natal'in, B.A., Sengor, A.M.C., 2005. Late Palaeozoic to Triassic evolution of the Turan and Scythian platforms: the pre-history of the palaeo-Tethyan closure. Tectonophysics 404, 175–202.

Passchier, C.W., Trouw, R.A.J., 2005. Microtectonics. Springer-Verlag, Berlin. 366 pp.

Perello, J., Cox, D., Garamjav, D., 2001. Oyu Tolgoi, Mongolia: Siluro-Devonian porphyry Cu–Au–(Mo) and high-sulfidation Cu mineralization with a Cretaceous chalcocite blanket. Economic Geology 96, 1407–1428.

Reiners, P.W., Brandon, M.T., 2006. Using thermochronology to understand orogenic erosion. Annual Reviews in Earth and Planetary Science 34, 419–466.

Renne, P.R., Swisher, C.C., Deino, A.L., Karner, D.B., Owens, T.L., DePaolo, D.J., 1998. Intercalibration of standards, absolute ages and uncertainties in 40Ar/39Ar dating. Chemical Geology 145, 117–152.

Ring, U., Brandon, M.T., Willett, S.D., Lister, G.S., 1999. Exhumation processes. In: Ring, U., Brandon, M.T., Lister, G.S., Willett, S.D. (Eds.), Exhumation Processes: Normal Faulting, Ductile Flow, and Erosion: Geological Society of London Special Publications, 154, pp. 1–27.

Ritts, B.D., Biffi, U., 2000. Magnitude of post-Middle Jurassic (Bajocian) displacement on the Altyn Tagh fault, NW China. Geological Society of America Bulletin 112, 61–74.

Ritts, B.D., Weislogel, A., Graham, S.A., Darby, B.J., 2009. Mesozoic tectonics and sedimentation of the giant polyphase nonmarine intraplate Ordos basin, western North China Block. International Geology Review 51, 95–115.

Roger, F., Jolivet, M., Malavieille, J., 2008. Tectonic evolution of the Triassic fold belts of Tibet. Comptes Rendus Geosciences 340, 180–189.

Ruzhentsev, S.V., Pospelov, I.I., 1992. The South Mongolian Variscan fold system. Geotectonics 26, 383–385.

Sengor, A.M.C., Natal'in, B.A., 1996. Paleotectonics of Asia: fragments of a synthesis. In: Yin, A., Harrison, M. (Eds.), The Tectonic Evolution of Asia. Cambridge University Press, Cambridge, pp. 486–640.

Sengor, A.M.C., Natal'in, B.A., Burtman, V.S., 1993. Evolution of the Altaid tectonic collage and Palaeozoic crustal growth in Eurasia. Nature 364, 299–307.

Steiger, R.H., Jäger, E., 1977. Subcommission on geochronology: convention on the use of decay constants in geo- and cosmochronology. Earth and Planetary Science Letters 36, 359–362.

Tapponnier, R., Peltzer, G., Le Dain, A.Y., Armijo, R., Cobbold, P., 1982. Propagating extrusion tectonics in Asia; new insights from simple experiments with plasticine. Geology 10, 611–616.

Taylor, J.P., Webb, L.E., Fitzgerald, P.G., Johnson, C.L., Heumann, M.J., 2008. Constraints on the low temperature thermal history of the Tsagan Subarga and Tavan Har basement blocks of the East Gobi Fault Zone, Southeastern Mongolia, and tectonic implication. 2008 Fall Meeting Supplemental Abstracts: Eos Transactions, AGU. T23C-2044.

Tomurtogoo, O., 1999. Geological Map of Mongolia. General Directorate of Mineral Research and Exploration, Ankara, Turkey.

Wang, T., Zheng, Y., Li, T., Gao, Y., 2004. Mesozoic granitic magmatism in extensional tectonics near the Mongolian border in China and its implications for crustal growth. Journal of Asian Earth Sciences 23, 715–729.

Wang, Y., Zhang, X., Wang, E., Zhang, J., Li, Q., Sun, G., 2005. 40Ar/39Ar thermochronological evidence for formation and Mesozoic evolution of the northern-central segment of the Altyn Tagh fault system in the northern Tibetan Plateau. Geological Society of America Bulletin 117, 1336–1346.

Watanabe, Y., Stein, H.J., 2000. Re–Os ages for the Erdenet and Tsagaan Suvarga porphyry Cu–Mo deposits. Economic Geology 95 (7), 1537–1542.

Webb, L.E., Johnson, C.L., 2006. Tertiary strike-slip faulting in southeastern Mongolia and implications for Asian tectonics. Earth and Planetary Science Letters 241, 323–335.

Xu, X., Harbert, W., Dril, S., Kravchinsky, V., 1997. New paleomagnetic data from the Mongol-Okhotsk collision zone, Chita region, south-central Russia, implications for Paleozoic paleogeography of the Mongol-Okhotsk ocean. Tectonophysics 269, 113–129.

Yue, Y., Liou, J.G., 1999. Two-stage evolution model for the Altyn Tagh Fault, China. Geology 27, 227–230.

Zonenshain, L.P., Kuzmin, M.I., Natapov, L.M., 1990. Geology of the USSR: Plate Tectonic Synthesis. American Geophysical Union.

Zorin, Y.A., 1999. Geodynamics of the western part of the Mongolia-Okhotsk collisional belt, Trans-Baikal region (Russia) and Mongolia. Tectonophysics 306, 33–56.

Please cite this article as: Webb, L.E., et al., Late Triassic sinistral shear in the East Gobi Fault Zone, Mongolia, Tectonophysics (2010), doi:10.1016/j.tecto.2010.09.033